Influence of network topology on sound propagation in granular materials

Danielle S. Bassett,[1,*] Eli T. Owens,[2] Karen E. Daniels,[2] and Mason A. Porter[3,4]

[1]*Department of Physics, University of California, Santa Barbara, California 93106, USA*

[2]*Department of Physics, North Carolina State University, Raleigh, North Carolina 27607, USA*

[3]*Oxford Centre for Industrial and Applied Mathematics, Mathematical Institute, University of Oxford, Oxford OX1 3LB, United Kingdom*

[4]*CABDyN Complexity Centre, University of Oxford, Oxford, OX1 1HP, United Kingdom*

Granular media, whose features range from the particle scale to the force-chain scale and the bulk scale, are usually modeled as either particulate or continuum materials. In contrast with each of these approaches, network representations are natural for the simultaneous examination of microscopic, mesoscopic, and macroscopic features. In this paper, we treat granular materials as spatially embedded networks in which the nodes (particles) are connected by weighted edges obtained from contact forces. We test a variety of network measures to determine their utility in helping to describe sound propagation in granular networks and find that network diagnostics can be used to probe particle-, curve-, domain-, and system-scale structures in granular media. In particular, diagnostics of mesoscale network structure are reproducible across experiments, are correlated with sound propagation in this medium, and can be used to identify potentially interesting size scales. We also demonstrate that the sensitivity of network diagnostics depends on the phase of sound propagation. In the injection phase, the signal propagates systemically, as indicated by correlations with the network diagnostic of global efficiency. In the scattering phase, however, the signal is better predicted by mesoscale community structure, suggesting that the acoustic signal scatters over local geographic neighborhoods. Collectively, our results demonstrate how the force network of a granular system is imprinted on transmitted waves.

PACS number(s): 81.05.Rm, 81.70.Cv, 89.75.Fb, 89.75.Hc

I. INTRODUCTION

During the past 15 years, techniques from areas of physics such as statistical mechanics and nonlinear dynamics have been used to make important advances in studying networks across myriad disciplines [1]. Conversely, the perspective of networks can also play important roles in physical problems, as there is a large class of heterogeneous systems—such as foams, emulsions, and granular materials [2,3]—for which the connectivity of the constituent elements is an important factor in the deviation of their behavior from continuum models. In fact, the discontinuous nature of granular materials led to the early idea of a fabric structure governing the anisotropic behavior of such materials [4–6].

We investigate whether studying the rich and complex dynamics of granular materials [7] using network analysis can provide new insights into the underlying physics. This treatment is a natural one, because granular materials can be represented as spatially embedded networks [8] composed of nodes (particles) and edges (contacts between particles) with definite locations in Euclidean space [9,10]. In Fig. 1, we show a quasi-two-dimensional granular system composed of photoelastic disks, which permits the determination of both the *contact network* and the interparticle forces. The forces between particles in these systems are nonhomogeneous, and they form a network of chain-like structures that span the system [see Fig. 1(b)]. This *force-chain network* has the same topology as the contact network but contains edges that are weighted by the interparticle forces [Fig. 1(c)]. This is exciting from a networks perspective, as it allows us to study the influence of network topology on "network geometry"

in a spatially embedded system. From the perspective of granular materials, earlier work suggests that force chains provide the main supporting structure for static and dynamic loading [11,12].

Because signal propagation in granular and heterogeneous materials [13] is of considerable importance to numerous industrial and natural systems, it has been the topic of many investigations. A longstanding question is how to reconcile the failure of continuum models of granular sound propagation [14–17], as such models that have been unable to quantitatively describe important heterogeneous and nonlinear features of acoustic speed [18–21]. The presence of force chains has been suggested as a potentially confounding phenomenon that might underlie the failure of previous physical models of sound propagation [18,22]. Ultimately, it would be beneficial to quantify how the pressure or strain state of a system is imprinted on transmitted waves and to understand how to use these waves to accurately detect buried objects or reservoirs of oil.

An increasing body of work has used tools from areas like network science and computational homology to obtain insights about the structural properties of granular materials [9,10,23] and other continuous media [24]. Indeed, a networks perspective provides a valuable complement to the standard ways of studying granular materials. In the present paper, we analyze experimental data using network analysis to investigate the role of force-weighted contact networks in sound propagation. The use of photoelastic particles combined with high-speed imaging allows us to gain insight into internal force structures and particle-scale sound propagation; such insights are not readily available when using ordinary granular materials. We find that geographic community structure provides a fundamental constraint to sound propagation, illustrating that contact topology alone is insufficient to understand signal propagation in granular materials.
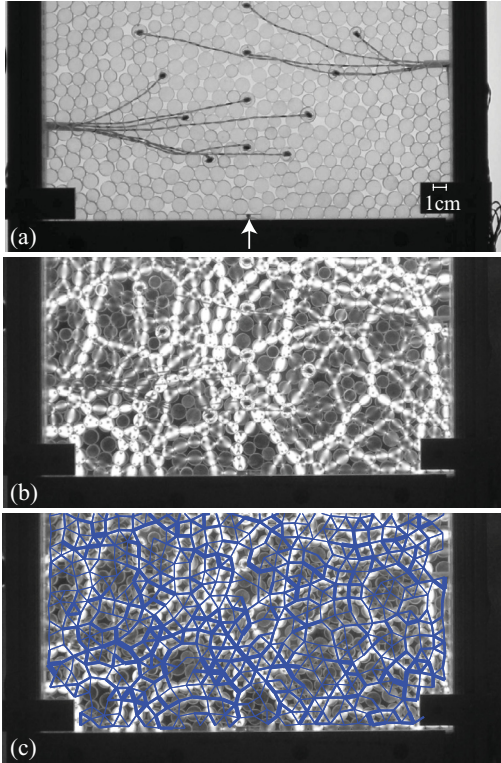
---

*dbassett@physics.ucsb.edu

FIG. 1. (Color online) (a) Image of a 2D vertical aggregate of photoelastic disks confined in a single layer. The driver position is marked with an arrow. Several particles are embedded with a piezoelectric sensor, for which wires are visible. (b) The internal stress pattern within the photoelastic particles manifests as a network of force chains. (c) The dark (blue) lines show a weighted graph, which is determined from image processing and overlaid on the image from panel (b). An edge between two particles (nodes) exists if the two particles are in physical contact with each other; the forces between particles give the weights of the edges.

II. EXPERIMENTS

We perform experiments on a vertical 2D granular system of bidisperse disks confined between two sheets of Plexiglas, which have been slightly lubricated with baking powder to reduce friction with the container walls. The top of the container is open, and the particles are confined exclusively by gravity. The particles are 6.35 mm thick, have diameters $d_1 = 9$ mm and $d_2 = 11$ mm, and are cut from Vishay PSM-4 photoelastic material to provide measurements of the internal forces. We show example images in Fig. 1. These particles have an elastic modulus of $E = 4$ MPa, and they are sufficiently dissipative that propagating sound waves experience an approximately exponential decay as a function of distance from the source. The use of such soft, dissipative particles differs from previous work [25–29], where much harder particles have been used. Further details about the apparatus are described in Ref. [22].

We excite acoustic waves from the bottom of the system by sending pulses of five 750 Hz sinusoidal waves with a voice coil driver attached to a 20 mm wide platform; maximum particle displacements are roughly 5 μm. To assess the reliability of network diagnostics, we repeat the experiments for 17 different particle configurations, each of which is

obtained by manual rearrangement. We restrict our analysis to a region of the system that contains just over $N = 400$ particles. This subsystem corresponds to a region in which vertical force gradients are minimized due to the Janssen effect [30].

We compute particle positions and forces using two high-resolution pictures of the static system and one high-speed movie that captures the system dynamics. We take one static image without the polarizer [see Fig. 1(a)] and use it to determine particle positions and contacts [22,31]. We take a second static image using polarizers [see Fig. 1(b)], and we use this image to estimate the normal forces at each contact [22]. In the vicinity of each contact, we use a combination of the light intensity (I), the square of the mean intensity gradient ($|\nabla I|^2$), and the position of the photoelastic fringes to estimate the contact forces by comparing them to calibration images with known forces. We measure the amplitude and location of sound propagation using a high-speed camera operating at 4000 Hz; the camera records 80 frames of data (20 ms) containing both the injection of the signal ($0 < t < 40$) and its dissipation ($40 < t < 80$). For each particle in each frame, we compute $\Delta I(x,y,t) = I(x,y,t) - I(x,y,t_0)$, which measures how much the brightness I of the particle changes with respect to its unperturbed brightness. In earlier work [22], we used piezoelectric sensors embedded in a subset of the particles to determine that ΔI is proportional to the change in stress on that particle. Using ΔI allows us to follow the propagating signal through all particles in the measurement region.

To determine which particles are in contact, we use the positions of the particle centers, which we determine from the static image of the system using a Hough transform. If the distance between two particle centers is less than 1.05 times the sum of their radii, we treat the particles as being in contact. This method overcounts the number of true contacts. However, the effect of such overcounting is minimized by the fact that false contacts are assigned a force value of almost zero when we apply our image-processing techniques to find the contact forces. Accordingly, they do not contribute significantly to the structure of the weighted network.

For each experimental run, we construct both an unweighted (binary) and a weighted network, which correspond respectively to an underlying contact network and a force-chain network (see Fig. 1). In each type of network, the nodes represent the particles in the system. In the binary network **A**, an edge exists between node i and j (i.e., $A_{ij} = 1$) if node i is in contact with node j; otherwise, $A_{ij} = 0$. The weighted network **W** contains the same edges, but each element W_{ij} now has a value that is given by an estimate of the normal force f_{ij} between particles i and j, normalized by the mean force $\overline{f}$ of all contacts: $W_{ij} = f_{ij}/\overline{f}$.

III. RESULTS

We assess the global organization of the networks using 21 candidate diagnostics for **A** and 8 candidate diagnostics for **W**. We define each diagnostic in Appendix A, where we also include descriptions to provide intuition about what each of them measures; these descriptions also indicate their possible physical significance to the granular system that we study. We examine the reliability of these diagnostics

across experimental runs in Appendix B, and we compare the binary network diagnostics to those in a null model constructed using an ensemble of random geometric graphs (RGGs) [32] in Appendix C. We examine four diagnostics (clustering coefficient, geodesic node betweenness, optimized modularity, and global efficiency) in further detail. Each of these four diagnostics can be defined for both binary and weighted networks, and each is helpful for obtaining insights into a particular type of spatial structure in the system: particles (clustering coefficient), curves (betweenness), mesoscale domains (via community structure determined from modularity optimization), and the entire system (global efficiency). We describe our results in the sections below.

A. Scale sensitivity of network diagnostics

A key advantage of using network tools to study granular materials is that different network diagnostics (which we define and discuss in detail in Appendix A) are sensitive to different system scales, and this is especially helpful for spatially embedded systems like granular packings (see Fig. 2). Our results indicate that the global efficiency E_w [see Eq. (A19)] is a system-level property that has its smallest values along the perimeter of the system and its largest values in the center. Community structure, and its associated community label X [see Eq. (A23)] and intracommunity strength z-score [see Eq. (3)], is a mesoscale property and can be used to probe intermediate structural features. We find that geodesic node betweenness B_w [see Eq. (A21)] can be construed as a one-dimensional property in these
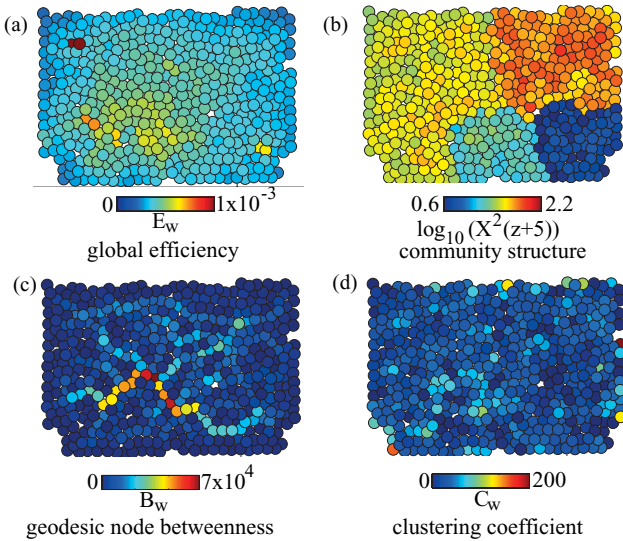

FIG. 2. (Color online) Example distributions of several network diagnostics for a sample granular packing. The network characteristics that we examine include (a) global efficiency E_w, (b) community structure, which we visualize using the quantity $X^2(z+5)$, where X is the community label, (c) geodesic node betweenness B_w, and (d) clustering coefficient C_w. This figure illustrates their respective sensitivities to system-scale (2D), domain-scale (2D), curve-scale (1D), and particle-scale (0D) structure. The quantity $X^2(z+5)$ allows us to visualize both the community label (X) and the intracommunity strength z-score z [see Eq. (3)] simultaneously; we chose the constant 5 purely for visual clarity.

materials because it is sensitive to curve-like structures in the network. Finally, we find that clustering coefficient C_w [see Eqs. (A9) and (A20)] is sensitive to particle-scale features of the network. In Sec. III D, we report how each of these network diagnostics correlates with sound propagation through the granular material.

B. Identifying a characteristic size scale

An ongoing challenge in the study of granular systems is identifying and measuring characteristic size scales within granular materials from the perspective of either particles or force chains [2,3,33]. Network modularity provides a novel means to measure such size scales via the identification of community sizes. We find that the optimal value of modularity is a reliable diagnostic for the structure of both the binary and weighted networks (see Appendix B). To seek characteristic community sizes, we also examine community structure as a function of a resolution parameter γ [34–36]. The modularity index for a weighted network **W** is [37]

$$Q_w = \sum_{ij}[W_{ij} - \gamma P_{ij}]\delta(g_i,g_j), \qquad (1)$$

where node i is assigned to community g_i, node j is assigned to community g_j, $\delta(g_i,g_j) = 1$ if $g_i = g_j$ and it equals 0 otherwise, and P_{ij} is the expected weight of the edge-connecting node i and node j under a specified null model. We use the usual Newman-Girvan null model, in which the expected strength distribution of the network is preserved [37,38]. We employ the Louvain locally greedy algorithm to optimize modularity [39], and we vary the resolution parameter γ from 0.001 to 1000. Low values of γ probe large spatial scales, and high values probe small scales. When we increase γ, the number of communities increases (as expected), and the modularity decreases. See Figs. 3(a) and 3(c).

One can think of the term $J_{ij}(\gamma) = W_{ij} - \gamma P_{ij}$ in Eq. (1) as a particular choice of interaction strength between a pair of spins in a Potts model [34,37,40]. We exploit this analogy with the Potts model to transform the resolution parameter γ so that it measures the effective fraction of antiferromagnetic edges $\xi(\gamma)$ in a network [41]. We define $l^W(\gamma)$ to be the number of negative elements of $\mathbf{J}(\gamma)$. The transformed resolution parameter is then

$$\xi(\gamma) = \frac{l^W(\gamma) - l^W(\Lambda_{min})}{l^W(\Lambda_{max}) - l^W(\Lambda_{min})} \in [0,1], \qquad (2)$$

where Λ_{min} is the largest number of negative entries $J_{ij}(\gamma)$ for which an N-node network forms a single community and Λ_{max} is the smallest number for which the network forms N communities of size 1.

We examine community structure as a function of the transformed resolution parameter $\xi(\gamma)$, which we vary between 0 and 1. The optimized modularity, the mean size of communities, and the variance in community size all change gradually for most of the $\xi(\gamma)$ range [see Figs. 3(b), 3(f), and 3(h)], although abrupt changes are evident for very low and very high values of $\xi(\gamma)$. The gradual change hints at an interesting size scale, which occurs in partitions that contain about 50–250 communities (with a characteristic size of roughly 2–8 particles). One possibility is that this size
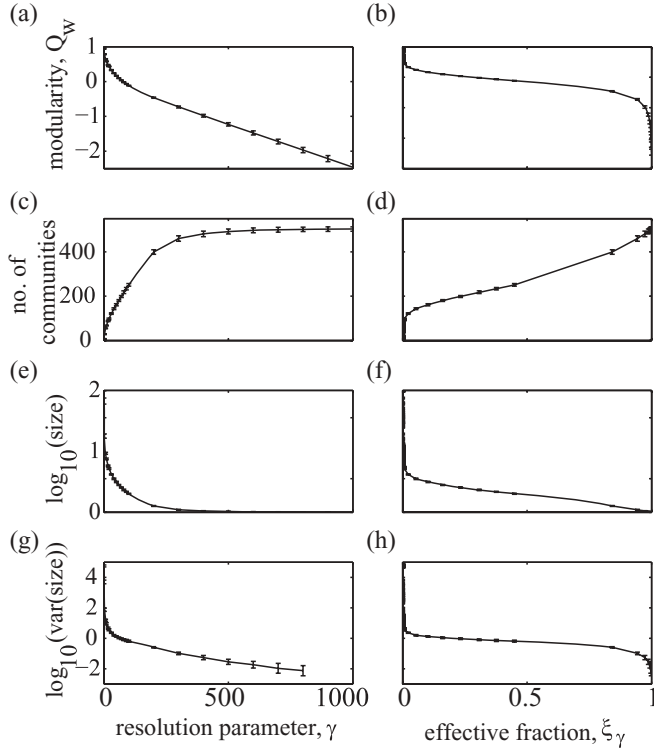
FIG. 3. (a), (b) Modularity index Q_w, (c), (d) number of communities, (e), (f) mean size of communities in terms of number of particles, and (g), (h) variance of community size as a function of (a), (c), (e), (g) the resolution parameter γ and (b), (d), (f), (h) the effective fraction of antiferromagnetic edges $\xi(\gamma)$. Error bars indicate the standard deviation over the 17 experimental runs.

corresponds to the width of a shear band. Such bands arise in a variety of materials with particulate structure [42]. Another possibility is that this size corresponds to the "cutting" length scale ℓ^* [43], which is set by a community size at which the excess (overconstrained) number of contacts in the bulk of a region is equal to the number of contacts around the perimeter. If this latter association is correct, then the mean number of particles per community would scale with the confining pressure. Future experiments can test this hypothesis.

C. Geography of community structures

Using modularity optimization [36–38,44], we find that the force-chain network exhibits geographically constrained community structure: Groups of particles in close spatial proximity are more likely to be a part of the same community (i.e., to contact one another with a large force) than particles that are farther apart. We examine this local neighborhood structure over a variety of size scales by varying the resolution parameter γ. We show representative results for large spatial scales in Figs. 4(a)–4(c). We also note that the communities that we identify in granular force networks resemble those in spatial entities like states or countries, whose borders are determined in part by physical boundaries between neighboring geographic domains.

Importantly, because the optimization of Q is NP-hard [45], one does not expect an optimization algorithm to give a

global optimum of Q. Instead, we harness numerous near-degeneracies [46] among good local optima of Q by estimating Q 100 times. We find that the these 100 values of Q for a given run at a given γ vary by approximately 1×10^{-14}, and the similarity in particle assignments to communities is approximately 0.98. We quantify this using partition similarity [47,48], which ranges from 0 (not similar at all) to 1 (identical). These results indicate that the local geographic structures that we are identifying in the 2D granular system are robust, suggesting the potential for identifying reproducible 2D "geographic" regions.

To probe the role of each particle in the community structure of a force-chain network [see Fig. 4(d)], we use the intracommunity strength z-score z_i to measure how well connected a node is to other particles in its community and the participation coefficient P_i to measure how the connections emanating from a particle are spread among particles in the different communities (including its own) [49].

The intracommunity strength z-score is

$$z_i = \frac{S_{g_i} - \bar{S}_{g_i}}{\sigma_{\bar{S}_{g_i}}}, \tag{3}$$

where S_{g_i} denotes the strength (i.e., the total edge weight) of node i's edges to other nodes in its own community g_i, the quantity $\bar{S}_{g_i}$ is the mean of S_{g_i} over all of the nodes in g_i, and $\sigma_{S_{g_i}}$ is the standard deviation of S_{g_i} in g_i. The (aggregate) strength of node i is denoted by S_i and gives the total force of all contacts on particle i.

The participation coefficient is [49]

$$P_i = 1 - \sum_{g=1}^{N_m} \left(\frac{S_{ig}}{S_i} \right)^2, \tag{4}$$

where S_{ig} is the strength of edges of node i to nodes in community g [49].

In Figs. 4(e) and 4(f), we show the intracommunity strength z-score and the participation coefficient for the community structure depicted in Fig. 4(a). Particles that are geographically central to a community tend to have higher values of z_i and lower values of P_i than particles at the geographic periphery of a community. From a physical perspective, z_i tends to be highest in particles with many force chains passing through them [compare, e.g., Figs. 4(d) and 4(g)], and high values of P_i are associated with the boundaries between communities (where there are few force chains).

We test whether the observed properties of community structure in our granular systems are related statistically to the interparticle forces that constitute the force-chain structure [see Figs. 4(d) and 4(g)] by examining the relationship between intracommunity strength z-score z_i, participation coefficient P_i, the normalized node strength $S_i' = S_i/N$, (i.e., the mean force of all edges emanating from a node), and the amplitude of the acoustic signal ΔI using the Spearman rank correlation coefficient ρ, which is defined as the Pearson correlation coefficient between ranked variables. We use the Spearman coefficient rather than the Pearson coefficient due to the non-normal distributions of ΔI values over particles.

We find that the mean force of all contacts on a particle (i.e., S_i') is significantly positively correlated with z_i [see Fig. 4(h)]. The mean value of the Spearman rank correlation coefficient
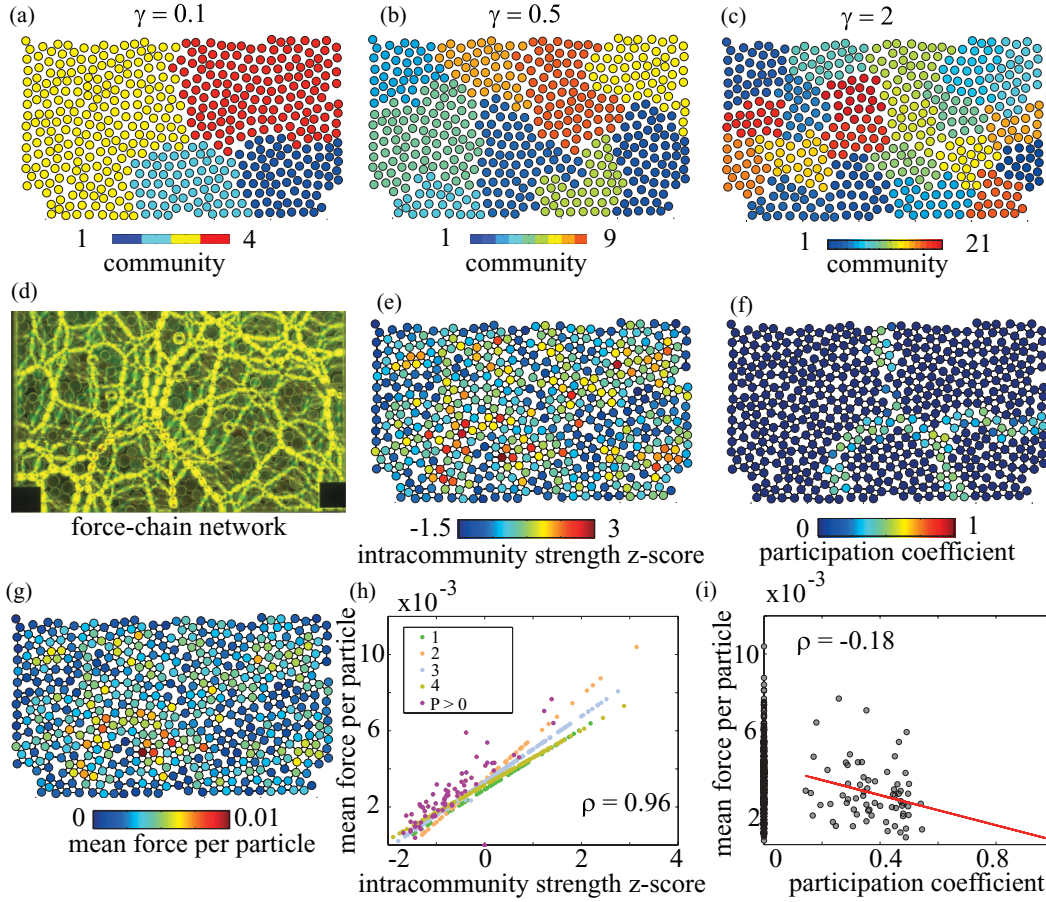
FIG. 4. (Color online) The geographic sizes of communities tend to decrease as the resolution parameter γ is increased from (a) $\gamma = 0.1$ to (c) $\gamma = 2$. We color particles according to their community label. One can examine community structure of the (d) force-chain network using geographic location, (e) intracommunity strength z-score z_i, (f) participation coefficient P_i, and (g) mean force per particle S_i'. (Recall that i labels the particle.) Example scatter plots for a single experimental run demonstrating that the mean force S_i' on particle i is (h) positively correlated with the intracommunity strength z-score (the Spearman correlation coefficient for this run is $\rho \approx 0.96$ and the p-value is $p \approx 1.9 \times 10^{-283}$) and (i) negatively correlated with the participation coefficient ($\rho \approx -0.18$ and $p \approx 1.8 \times 10^{-5}$). Note that the correlations reported in panels (h) and (i) are for the resolution-parameter value of $\gamma = 0.1$. In panel (h), we display the nodes that are assigned to communities 1 through 4 and nodes whose participation coefficients are equal to 0 using different colored markers. We display nodes in any of the four communities whose participation coefficients are greater than 0 (so-called *boundary nodes*) using dark (purple) markers. The mean correlations for intracommunity strength z-score and participation coefficient over experimental runs and values of the resolution parameter are $\rho \approx 0.72 \pm 0.02$ and $\rho \approx -0.05 \pm 0.04$, respectively. We show the results for one experimental run (No. 2) in this figure, and the results for the other runs are similar.

ρ over experimental runs and resolution-parameter values is $\rho \approx 0.71 \pm 0.02$ (where 0.02 gives the standard deviation over experimental runs). This strong positive correlation indicates that particles at the centers of communities are likely to have more or stronger force chains running through them. We also find that S_i' is negatively correlated with P_i [Fig. 4(i)]. The mean ρ over experimental runs and values of the resolution parameter is $\rho \approx -0.05 \pm 0.04$, where we again take the standard deviation only over experimental runs. As γ is increased, ρ changes from negative to positive, and the mean over γ values is near 0. Note additionally that a large fraction of the particles have participation coefficients of 0. This is a consequence of the fact that the communities are geographically constrained such that the majority of particles have contacts only within their own community.

The relationships between z, P, and S' are expected. For example, if the edges of node i all lie within its own community, then S' and z are related linearly according to the following equation: $S_i = z_i \sigma_{S_{g_i}} + \bar{S}_{g_i}$, where we recall that S_{g_i} is the strength of edges of node i to other nodes in its community g_i, and $\bar{S}_{g_i}$ is the mean of S_{g_i} over all of the nodes in g_i. This linear relationship is evident for the four communities that we show in Fig. 4(h). Nodes whose connections span more than one community (so-called *boundary nodes*, for which the value of P is greater than 0) are not so simply related.

D. Signal propagation on force-weighted contact networks

Previous work in Ref. [22] has shown that the propagation of acoustic signals is facilitated along strong force chains in granular materials via the increased contact area at strong contacts. With this in mind, we test whether the geographic
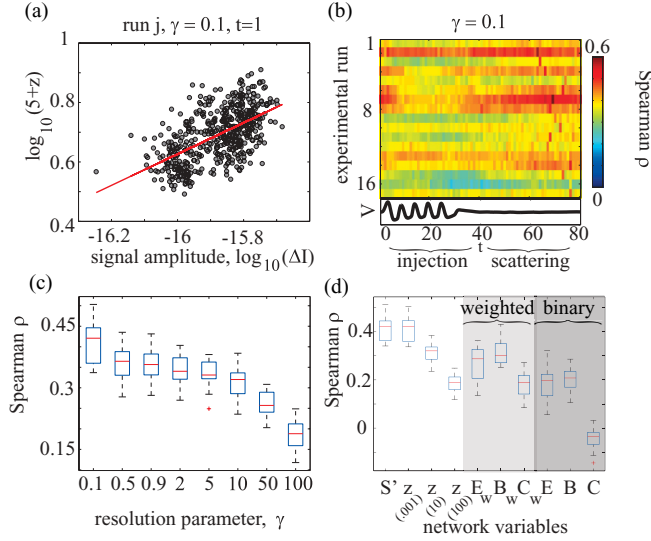
FIG. 5. (Color online) (a) An example scatter plot between logarithms of the intracommunity strength z-score [$\log_{10}(z+5)$] and the amplitude of the acoustic signal [$\log_{10}(\Delta I)$] at $t=1$ for a single experimental run ($j=2$) and resolution-parameter value ($\gamma = 0.1$). We added the constant 5 to z to ensure that all values were positive prior to taking the logarithm. The Spearman rank correlation coefficient is $\rho \approx 0.57$ and the p-value is $p \approx 2.1 \times 10^{-45}$. (b) Correlation between $\log_{10}(z+5)$ and $\log_{10}(\Delta I)$ for all 17 runs as a function of time: $t < 40$ is the acoustic signal injection phase, and $t > 40$ is the acoustic signal scattering phase. In the bottom part of panel (b), we show a trace of the voltage V of a piezo particle; the injected signal has an amplitude of 0.5V. (c) Correlation between $\log_{10}(z+5)$ and $\log_{10}(\Delta I)$ as a function of γ, where $\gamma \in [0,2]$ is increased in increments of 0.1. We averaged the correlation over all 80 time points at which ΔI was measured. The mean ρ over runs, γ values, and time was 0.34 ± 0.06. Box plots show the variability over experimental runs. (d) Correlation between $\log_{10}(\Delta I)$ and a variety of network diagnostics: intracommunity strength z-score $z = z(\gamma)$ for $\gamma = 0.001$, $\gamma = 10$, and $\gamma = 100$ (white background, left part of the figure); and weighted (light gray background, middle part of the figure) and unweighted (dark gray background, right part of the figure) versions of global efficiency [$E_w(i)$ and $E(i)$], geodesic node betweenness [$B_w(i)$ and $B(i)$], and clustering coefficient [$C_w(i)$ and $C(i)$]. For completeness, we also show results for the mean force S' (left part of the figure), which was the variable previously reported to be correlated with ΔI [22].

community structure of force-chain networks is related to signal propagation. As the example shown in Fig. 5(a) indicates, we find that z, which we measure over a range of size scales associated with resolution-parameter values $\gamma \in [0.001, 100]$, is significantly correlated with the signal amplitude ΔI. (For this example run, $\rho \approx 0.57$ and the p-value is $p \approx 2.1 \times 10^{-45}$.) The statistical correlation between network structure and signal amplitude exists not only in the highly heterogeneous signal injection phase, in which sound propagates from the driver to nearby particles, but also in the more homogeneous scattering phase, in which sound reverberates throughout the system. In Fig. 5(b), we show the results at $\gamma = 0.1$. Figure 5(c) shows that the mean ρ over runs, γ values, and time is 0.34 ± 0.06. We discuss the dynamics within the injection and scattering phases in more detail in the next section.

In quantifying the relationship between the intracommunity strength z-score z (a property of the algorithmically computed community structure) and the signal propagation amplitude ΔI, we note that the correlation between these two variables decreases as γ increases [see Fig. 5(c)]. The strength of the relationship between network structure and signal propagation for small γ suggests that partitions with a few large communities have a greater association with the propagation behavior. Indeed, as demonstrated in Fig. 5(d), when the network forms a single community (for very low γ values), the correlation between z and ΔI is similar to that between the mean force per particle (S') and ΔI.

The retention of a correlation between z and ΔI for larger values of γ, for which the network is partitioned into more (and smaller) communities, stems from the strong correlation between intracommunity strength z-score and the mean force (normalized strength) of a particle [see Fig. 4(h)], the latter of which is a particle-scale measurement and is independent of spatial resolution. The relationship between the mesoscale (community structure) and particle-scale (mean force on a particle, which is equal to a node's normalized strength) network properties stems from the physical embedding of the granular system in $\mathbb{R}^2$. A particle that is located geographically inside of a community has all of its connections to other particles in its community because it is constrained to connect only to its geographic neighbors (i.e., there can be no long-range contacts). This is unlike most investigated real-world networks [36,37], in which communities tend to be highly interconnected and most nodes have at least some connections to nodes in other communities.

To assess whether community structure is unique in its ability to predict signal amplitude, we also examine other weighted network diagnostics that are sensitive to different system dimensionalities (see Fig. 2). Our results suggest that community structure [see Fig. 2(b)] is a better predictor of signal propagation than system-scale [e.g., global efficiency; see Fig. 2(a)], curve-scale [e.g., geodesic node betweenness; see Fig. 2(c)], and particle-scale [e.g., clustering coefficient; see Fig. 2(d)] network diagnostics. See Appendix A for mathematical definitions and intuitive descriptions. In particular, clustering coefficient and ΔI are not strongly correlated, so triangles of contacts do not appear to be important for signal propagation. See the comparison in Fig. 5(d).

E. Phase sensitivity of network diagnostics

Although the correlation between z and signal amplitude is strong in both injection and scattering phases for small γ (i.e., large community size), it is higher in the scattering phase than in the injection phase when averaged over all resolutions [$\gamma \in [0.001, 1000]$; see Figs. 6(b) and 6(e); we indicate the specific values of γ in the figure caption]. We do not observe such sensitivity to phase for the mean force per particle [see Figs. 6(a) and 6(d)]. Interestingly, the signal propagation during the injection phase is more strongly correlated with the global efficiency than it is during the scattering phase [see Figs. 6(c) and 6(f)], suggesting that the acoustic signal propagates over the shortest weighted paths during the injection phase. These results illustrate insights from network analysis that one cannot obtain from particle-scale
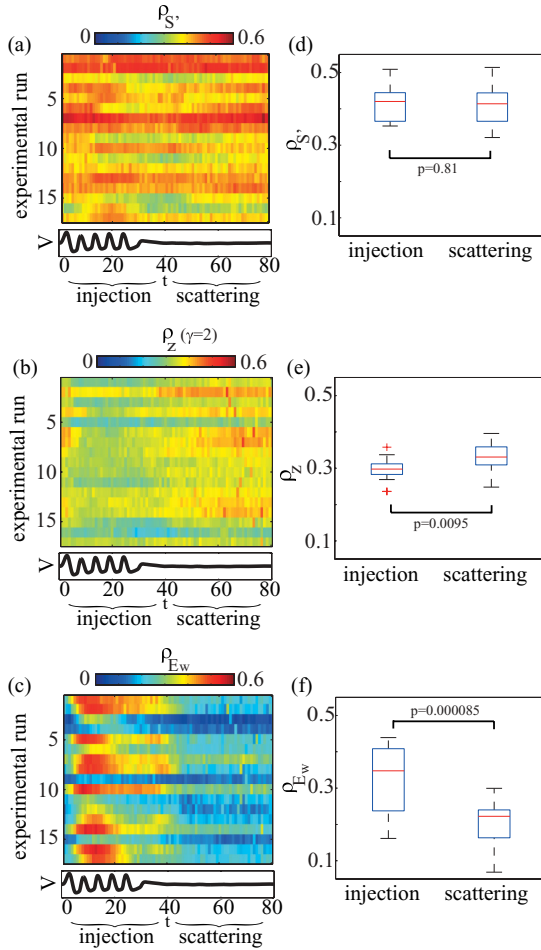
FIG. 6. (Color online) Spearman correlations between signal amplitude ΔI and (a) the mean force per particle S', (b) the intracommunity strength z-score z for $\gamma = 2$, and (c) the global efficiency E_w. Our data encompass all experimental runs and all times, including both injection (left) and scattering (right) phases. We show the Spearman correlations between signal amplitude ΔI and the three diagnostics shown in panels (a)–(c) in box plots: (d) mean force per particle ($\rho_{S'}$), (e) intracommunity strength z-score z (ρ_z), and (f) global efficiency (ρ_{E_w}). We have averaged the correlations that we show in the box plots separately over the injection (left) and scattering (right) phases. For panel (e), note that we also average the correlations over the resolution parameter γ. Using MATLAB notation, the precise values of γ that we considered are $[0.001 : 0.001 : 0.009, 0.01 : 0.1 : 0.91, 2, 3, 4 : 0.1 : 20, 30 : 10 : 100, 200 : 100 : 1000]$. The reported p-values indicate the results of two-sample t-tests.

measurements: Signal propagation during injection is well characterized by shortest paths that span the system, whereas it is characterized by local neighborhood structure during scattering. An interesting question is whether the amplitude of the injected signal affects the size of the geographic neighborhood through which it propagates.

We also examine the sensitivity of the relationship between z and ΔI to the injection and scattering phases as a function of the resolution parameter [see Fig. 7(a)]. The correlation between z and signal amplitude is consistently higher in the scattering phase than in the injection phase throughout $\gamma \in [0.001, 1000]$. Furthermore, the largest difference in the
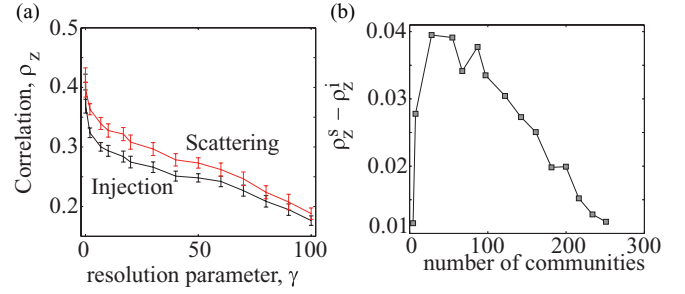

FIG. 7. (Color online) (a) Spearman correlations between signal amplitude ΔI and the intracommunity strength z-score z averaged over the injection (lower; black) and scattering (upper; red) phases as a function of the resolution parameter γ. (b) Difference between the correlation in the scattering (ρ_z^s) and injection (ρ_z^i) phases as a function of the number of communities in the partition. We find the greatest sensitivity to phase for partitions with approximately 50–100 communities (i.e., for communities containing roughly five to eight particles), which corresponds to the upper end of the size scale (two to eight particles) that we identified as potentially interesting using the transformed resolution parameter.

Spearman correlation between z and ΔI for the scattering versus injection phases occurs for partitions with approximately 50–100 communities, corresponding to community sizes of roughly five to eight particles [see Fig. 7(b)]. This is similar to the size scale that we identified previously when using the transformed resolution parameter.

IV. DISCUSSION

A networks perspective provides a useful framework in which to study the material and dynamic properties of granular materials. Network diagnostics vary in their sensitivity to scales of the granular system: The particle scale can be probed with a clustering coefficient, the curve scale can be probed with geodesic node betweenness, the domain scale can be probed with community structure, and the system scale can be probed with global efficiency. Moreover, one can identify potentially interesting length/size scales in the system using mesoscale network features such as community structure. As we show in Appendix A, one can also obtain physical insights into the geographic organization of the material by comparing the features of the actual networks to a null model consisting of an ensemble of random geometric graphs.

The dynamics of signal propagation on a network are best characterized by weighted diagnostics derived from the granular force-chain network, suggesting that the topology of the underlying (unweighted) contact network alone is not sufficient to explain signal propagation. In other words, one must also consider network geometry. This result underscores the important relationship between signal propagation and force-chain organization [see Fig. 5(d)]. Similar phenomena are likely relevant for a variety of energy transport problems (e.g., in sound, heat, and electricity) in a broad class of amorphous materials. Although real 3D granular systems are not photoelastic, recent advances in tomography [50,51] have begun to provide data on contact forces within packings of deformable spheres. As experimental techniques mature, it will be possible to apply network analyses to laboratory 3D systems.

The algorithmic detection of communities is particularly useful in quantifying the effect of mesoscale network structure on signal propagation. We find that community structure is a better predictor of signal amplitude over the range of propagation phases than system-scale, curve-scale, or particle-scale measurements. Furthermore, by contrasting signal behavior during injection and scattering phases, we are able to differentiate the sensitivities of system-wide and mesoscale network structure to sound propagation. Community structure seems to be a better predictor of signal propagation in the scattering phase than in the injection phase, suggesting that the sound scatters in local geographic neighborhoods. However, global efficiency predicts signal propagation better in the injection phase than in the scattering phase, suggesting a more system-wide dynamic distribution of sound.

Studying community structure allows one to investigate the mesoscale architecture of granular packings. In addition to the intracommunity strength z-score predicting particle-scale sound amplitude, the identification of geographic communities provides a quantifiable size scale, which might be useful for seeking the diverging length scale that is expected at the jamming transition [2,3]. The mesoscale nature of the sound propagation might be related to other mesoscale phenomena in granular physics, such as the spatial eigenmodes for soft (low-energy) modes, which are observed in simulations to take the form of localized swirls [52,53]. Our approach also provides a framework to relate 1D structures (force chains) to 2D structures (geographic domains). It therefore might also prove useful in other settings, such as in the study of crystalline solids, where domain structure is critical to system function.

The presence of correlated regions such as geographic communities in a granular material is reminiscent of shear transformation zones (STZs) [54], in which localized regions throughout a sheared material have an increased propensity to deform under shear. Importantly, however, the community structure that we compute spans the system, whereas STZs are relatively small structures dispersed throughout a system. Also of interest is a comparison with the results of Ref. [55], which illustrated that vibrational modes can identify soft spots in sheared systems.

In conclusion, using network analysis to study granular materials can be extremely useful, as it can help characterize particle-, curve-, domain-, and system-scale properties in such media. In particular, the algorithmic detection of communities provides a means to identify potentially interesting characteristic size scales in such systems. When combined with time-resolved acoustic measurements [22], such a networks perspective can help illuminate mesoscale structures within which sound travels preferentially. We find that particles that are well connected to their community have larger-amplitude signals passing through them. Our results also suggest that signals scatter in local geographic neighborhoods but propagate more systemically during signal injection. Investigation of both weighted and unweighted networks demonstrates that a weighted network is a better predictor of sound propagation, suggesting that the force-chain structure of the granular material is an important component in sound propagation. Our results show that one cannot examine only system-scale or local-scale network features to understand how sound travels through a granular material. Importantly, one achieves a better description of sound propagation when one includes how the particles relate to their neighbors in a network.

APPENDIX A: DEFINITIONS OF NETWORK DIAGNOSTICS

1. Diagnostics applied to unweighted contact networks

To characterize structure in the binary (contact) networks, we examined 21 diagnostics: number of nodes, number of edges, global efficiency [56], geodesic node betweenness centrality [57,58], random-walk node betweenness [59], geodesic edge betweenness [60], eigenvector centrality [61], closeness centrality [62], subgraph centrality [63], communicability [64,65], clustering coefficient [66], local efficiency [56], modularity optimized using two different algorithms [37–39,44], hierarchy [67], synchronizability [68], degree assortativity [69], robustness to targeted and random attacks [70], the Rent exponent [71], and mean connection distance [72].

In our descriptions below, we give for each diagnostic (i) a mathematical definition, (ii) an intuitive description of the term, and (iii) a comment on its possible physical significance for the granular system that we study. We also compute node-specific values for the following diagnostics: geodesic betweenness, global efficiency, and clustering coefficient. (See the discussions below.)

(1) Number of nodes N: (i) The diagnostic N is defined as the number of nodes in a network. (ii) It is used as a measure of the size of a system. (iii) In this study, N is the number of particles in the system. It provides a consistent but dynamically uninteresting characterization of the network because it is identical at all points in time.

(2) Number of edges D: (i) The diagnostic D is defined as $D = \sum_{ij} A_{ij}$, where $\mathbf{A}$ is an unweighted (binary) network with components A_{ij}. Nodes are particles, and an edge exists between particles i and j (i.e, $A_{ij} = 1$) if and only if particles i and j are in contact with each other (otherwise, $A_{ij} = 0$). (ii) The quantity D is simply the total number of edges in the system. (iii) The number of edges D is related to the mean contact number, which is denoted by z in the granular-materials community. The mean contact number of the system is equal to $z = \frac{D}{2N}$. The diagnostic D provides a consistent but uninteresting characterization of the network because the

number of contacts scales with pressure [2] (which is the same for all experimental runs).

(3) *Global efficiency* E [56]: (i) Let d_{ij} be the shortest (geodesic) number of steps necessary to get from node i to node j. The global efficiency is then defined as

$$E = \frac{1}{N(N-1)} \sum_{i \neq j} \frac{1}{d_{ij}} . \qquad (A1)$$

(ii) Global efficiency can be interpreted as a measure of how well a signal is transmitted through a network. (iii) One can expect the global efficiency to be small in 2D granular packings because particles that are not geographically close to one another are separated by multiple contacts (edges) and therefore by a long path length (low efficiency). As one can see in Table III, this is indeed the case.

(4) *Geodesic node betweenness* B [57]: (i) Geodesic node betweenness is defined for the ith node in a network $\mathcal{G}$ as

$$B_i = \sum_{j,m,i \in \mathcal{G}} \frac{\psi_{j,m}(i)}{\psi_{j,m}}, \qquad (A2)$$

where all three nodes (j, m, and i) must be different from each other, $\psi_{j,m}$ is the number of geodesic paths between nodes j and m, and $\psi_{j,m}(i)$ is the number of geodesic paths between j and m that pass through node i. The geodesic betweenness of an entire network B is defined as the mean of B_i over all nodes i in the network. (ii) Geodesic betweenness can be interpreted as a measure of traffic flow on a network. (iii) One might expect the majority of geodesic paths that link any node of the packing to any other node to pass through the middle of the system. Indeed, we find that the largest values of betweenness occur in the center of the system and the smallest values occur along the edges of the packing.

(5) *Random-walk node betweenness* B_{rw} [59]: (i) For an adjacency matrix $\mathbf{A}$ and diagonal matrix $\mathbf{D}$, let $\mathbf{M}_t = \mathbf{A}_t \cdot \mathbf{D}_t^{-1}$ be the matrix $\mathbf{M}$ with row and column t removed (and $\mathbf{A}_t$ and $\mathbf{D}_t$ are defined analogously). The probability that a walk starts at node s, takes n steps, and ends up at some node i (which cannot be t because t has been removed) is given by element is of $\mathbf{M}_t^n$; denote this element by $[\mathbf{M}_t^n]_{is}$. Walks end up at v and w with probabilities $[\mathbf{M}_t^n]_{vs}$ and $[\mathbf{M}_t^n]_{ws}$, respectively. Fractions $1/k_v$ and $1/k_w$ of these walks subsequently pass along the edge (v,w) in one direction or the other, assuming that such an edge exists. (Note that k_v is the degree of v and k_w is the degree of w.) Summing over all n shows that the mean number of times that a walk of any length traverses the edge from v to w is $k_v^{-1}[(\mathbf{I} - \mathbf{M}_t)^{-1}]_{vs}$. (As discussed in Ref. [59], this expression does not depend on w.) The random-walk betweenness of a node is the mean of this quantity over all edges emanating from that node, and the random-walk betweenness of the entire network is the mean of the random-walk betweenness of all nodes in the network. (ii) Random-walk betweenness can be interpreted as a measure of information flow or signal flow in a network. (iii) Similar to geodesic node betweenness, one might expect the random walk node betweenness to be highest in the center of the system and lowest on the edges of the system. This is indeed the case.

(6) *Geodesic edge betweenness* B_e [60]: (i) Inspired by Freeman's geodesic node betweenness, the geodesic betweenness of an edge is defined as the number of shortest paths between pairs of nodes that run along it. For the edge that connects nodes j and m, the geodesic edge betweenness is given by

$$B_e(j,m) = \sum_{i,k} \psi_{i,k}(j,m), \qquad (A3)$$

where $\psi_{i,k}(j,m)$ is the number of shortest paths between i and k that pass through the edge that connects nodes j and m. (ii) One can interpret edge betweenness as a measure of the influence of an edge on traffic flow through a network. (iii) In a 2D granular packing, edge betweenness might indicate the influence of a contact on a hypothetical flow through the network. In our system, we find that edge betweenness is largest in the center of the system and smallest on the edges of the system. This is consistent with the results for geodesic node betweenness.

(7) *Eigenvector centrality* C_e [73]: (i) The eigenvector centrality $C_e(i)$ of node i is proportional to the sum of the eigenvector centralities of the nodes connected to it:

$$C_e(i) = \frac{1}{\lambda} \sum_{j \in M(i)} C_e(j) = \frac{1}{\lambda} \sum_{j} A_{ij} C_e(j), \qquad (A4)$$

where $M(i)$ is the set of nodes that are neighbors of i (i.e., which are connected to i directly via an edge) and λ is the largest eigenvalue of $\mathbf{A}$. From Eq. (A4), one can deduce that $C_e(i)$ is the ith component of the leading eigenvector (each entry of which is positive by the Perron-Frobenius theorem [1]) of the adjacency matrix. (ii) Eigenvector centrality can be used to measure the importance of a node in a network based on its direct connection to important nodes. (iii) In a 2D granular packing, one would expect eigenvector centrality to be large for a particle that has many contacts or for a particle whose immediate neighbors have many contacts. Indeed, we find that eigenvector centrality is highest in a local region of the system in which high-degree nodes are most concentrated.

(8) *Closeness centrality* C_c [62]: (i) We use a version of closeness centrality that is appropriate for both connected and disconnected graphs [74]. It is defined as

$$C_c(i) = \sum_{j \in V/i} 2^{-\psi_{\mathcal{G}}(i,j)}, \qquad (A5)$$

where $\psi_{\mathcal{G}}(i,j)$ is the geodesic distance between nodes i and j (i.e., the length of the shortest path connecting i and j) and the notation V/i indicates that V is the connected network component reachable from i and does not include i. (ii) Closeness centrality can be used as a measure of the importance of a node in a network. (iii) For 2D granular systems, one might expect closeness centrality to be small, given the lattice-like topology of a contact network. However, as shown in Table III, closeness values are somewhat larger than those for random geometric graphs (RGGs; see the discussion in Appendix C).

(9) *Subgraph centrality* C_s [63]: (i) We first note that the number of closed walks of length k starting and ending at node i is given by the kth local spectral moment $\mu_k(i)$, which is defined as the ith diagonal entry of the kth power of the

adjacency matrix $\mathbf{A}$:

$$\mu_k(i) = [\mathbf{A}^k]_{ii} . \tag{A6}$$

The subgraph centrality of node i is then defined as

$$C_s(i) = \sum_{k=0}^{\infty} \frac{\mu_k(i)}{k!} . \tag{A7}$$

(ii) Subgraph centrality characterizes the participation of each node in all subgraphs in a network. (iii) For 2D granular systems, one might expect subgraph centrality to be small because nodes participate in few subgraphs that are far away from them, as their connectivity is strongly constrained to their local geographic neighborhood. Indeed, as indicated in Table III, subgraph centrality has a value that is less than 1/3 of the value that we computed for a corresponding ensemble of RGGs (see our later discussion).

(10) Communicability C_o [64,65]: Because of the direct relationship between the powers of the adjacency matrix $\mathbf{A}$ and the number of walks in a network, one can define the communicability between nodes i and j as

$$C_{o_{ij}} = \sum_{k=0}^{\infty} \frac{[\mathbf{A}^k]_{ij}}{k!} . \tag{A8}$$

The communicability C_o of a network is then the mean of the communicabilities of each pair of (nonidentical) nodes. (ii) Communicability was developed to measure the ease of communication or transmission in terms of passage between different nodes in a network, and it is specifically based on walks rather than paths [64]. (iii) For 2D granular systems, one might expect the mean communicability to be small because the geographic nature of the contacts creates a lattice-like topology. Indeed, as indicated in Table III, its value is less than 1/4 of the value that we computed for a corresponding ensemble of RGGs.

(11) Clustering coefficient C [66]: (i) The diagnostic C is defined by supposing that a node i has k_i neighbors, so a maximum of $k_i(k_i - 1)/2$ edges can exist between these neighbors. The local clustering coefficient C_i is the fraction of these possible edges that actually exist:

$$C_i = \frac{\sum_{mj} A_{mj} A_{im} A_{ij}}{k_i(k_i - 1)} . \tag{A9}$$

The clustering coefficient C of an entire network is then defined as the mean of C_i over all nodes i. (ii) The clustering coefficient C can be interpreted as a measure of local clustering properties in a network. (iii) One can expect C to be large in 2D granular packings because particles that are geographically close to one another are also near each other in a network. This ought to yield a large number of connected triples and hence a high value of C. As shown in Table III, we do indeed observe reasonably large values [75] for clustering coefficients in the 17 experimental runs (the mean value over all runs is $C \approx 0.26$), but interestingly the mean value of C in the corresponding RGG ensemble is twice as high.

(12) Local efficiency E_l [56]: (i) The local efficiency of node i is defined as

$$E_l(i) = \frac{1}{N_{G_i}(N_{G_i} - 1)} \sum_{j,k \in G_i} \frac{1}{d_{j,k}}, \tag{A10}$$

where G_i is the subgraph consisting of all nodes connected to node i along with all of their edges between each other, and $d_{j,k}$ is the minimum path length between nodes j and k in this subgraph. The local efficiency E_l is the mean value of $E_l(i)$ over all nodes i. (ii) Local efficiency E_l can be interpreted as a measure how well a signal is transmitted through a subgraph. (iii) One might expect local efficiency to be large in 2D granular packings because particles that are very close to each other geographically lie in one another's subgraphs. However, as we show in Table III, we obtain values that are only about half of those for corresponding RGGs. The mean granular-network value of 0.33 is comparable in value to some communication networks [56].

(13) Modularity index Q [36–38]: (i) Networks can be partitioned into communities (or modules) in which nodes inside the same community are more densely connected to each other than they are to nodes in other communities. The modularity of a network partition is defined as

$$Q = \frac{1}{2D} \sum_{ij} \left[A_{ij} - \frac{k_i k_j}{2D} \right] \delta_{g_i, g_j}, \tag{A11}$$

where k_i is the degree of node i, D is the total number of edges in the network, δ_{ij} is the Kronecker delta, and g_i is the community to which node i has been assigned. With the standard null model $P_{ij} = k_i k_j/(2D)$, Eq. (A11) is sometimes called "Newman-Girvan modularity." One uses one of numerous possible computational heuristics to maximize Q in the space of all network partitions, and one can then report the maximum value obtained for Q. However, it is important to note that the optimization of Q is NP-hard [45], so one cannot expect the output of an optimization algorithm to be a globally optimal partition of a network. In this light, we use two different computational heuristics to optimize Q: Newman's spectral algorithm [44] implemented in the Brain Connectivity Toolbox [90] (which yields a modularity value that we denote Q_s) and the Louvain locally greedy method [39] (yielding a modularity value that we denote Q_L). (ii) The optimal value of Q is a measure of how well a network can be partitioned into cohesive communities. (iii) In a 2D granular system, one might expect communities to be localized geographically because connectivity between nodes in potential communities is constrained geographically. Indeed, as shown in Table III, the values of Q_s and Q_L are both extremely high [36,37].

(14) Hierarchy h [67]: (i) A sense of hierarchical structure in a network can be characterized by the coefficient h, which is used to quantify a putative power-law relationship between clustering coefficient C_i and the degree k_i of all nodes in the network [67]:

$$C_i \sim k_i^{-h} . \tag{A12}$$

(ii) Networks in which the clustering coefficient has a power-law scaling with degree possess a hierarchy in which hubs (i.e., high-degree nodes) tend to have low local clustering

and low-degree nodes tend to have high local clustering. The parameter h gives a precise scaling of such effects when (A12) holds, and it can perhaps indicate a looser sense of hierarchy in more general situations. (iii) It is not clear *a priori* whether 2D granular packings have some hierarchical characteristics, though the authors of Ref. [67] have suggested that geographic networks are not very hierarchical. Our calculations (see Table III) provide some support for this claim, as we observe that this scaling relationship between C_i and k_i seems to hold in our data and we obtain $h \approx 0.76$. It is noteworthy, however, that this value is roughly three times what one obtains in a corresponding RGG ensemble (see Table III).

(15) Synchronizability s [68]: (i) Synchronizability is defined as

$$s = \frac{\lambda_2}{\lambda_N},\tag{A13}$$

where λ_2 is the second smallest eigenvalue of the Laplacian $\mathcal{L} = \mathbf{D_A} - \mathbf{A}$ (where $\mathbf{D_A}$ is a diagonal matrix whose diagonal entries are the row sums of the corresponding row of $\mathbf{A}$) of the adjacency matrix and λ_N is the largest eigenvalue of $\mathcal{L}$ [68]. (ii) The synchronizability of a network characterizes structural properties of a network that hypothetically enable it to synchronize rapidly. (iii) One might expect that the synchronizability of the contact network in a 2D granular packing is small due to the lattice-like nature of the network topology. Indeed, as shown in Table III, the value for s for our system is tiny.

(16) Degree assortativity a [69]: (i) The degree assortativity of a network (which is often called simply "assortativity") is defined as

$$a = \frac{D^{-1} \sum_i j_i k_i - \left[D^{-1} \sum_i \frac{1}{2}(j_i + k_i) \right]^2}{D^{-1} \sum_i \frac{1}{2}\left(j_i^2 + k_i^2 \right) - \left[D^{-1} \sum_i \frac{1}{2}(j_i + k_i) \right]^2},\tag{A14}$$

where j_i and k_i are the degrees of the nodes at the two ends of the ith edge ($i \in \{1, \ldots, D\}$ [44]. (ii) Degree assortativity measures the preference of a node to connect to other nodes of similar degree (leading to an assortative network, for which $a > 0$) or to nodes of very different degree (leading to a disassortative network, for which $a < 0$). (iii) It is not clear *a priori* whether 2D granular packings should display degree assortativity. Our calculations indicate that the degrees exhibit some mild positive assortativity ($a \approx 0.14$), but the corresponding RGG ensembles have a significantly higher positive assortativity of $a \approx 0.56$ (see Table III).

(17) Robustness R [70]: (i) One can define robustness in terms of different types of attacks on a network. In the most commonly studied type of targeted attack, nodes are removed (one by one) in descending order of their degree; in a random attack, nodes are removed in random order (e.g., uniformly at random, which is what we consider). Each time a node is removed from a network, we recalculate the size S (i.e., number of nodes) of the largest connected component. One can examine robustness by plotting S versus the number of nodes n removed [76–78]. One can then define a robustness parameter R as the area under the curve in the plot of $S = S(n)$. More robust networks retain a larger connected component even when several nodes have been removed; this is represented by

a larger area under the curve and hence by larger values of R. (ii) Robustness indicates network resilience to either targeted (R_t) or random (R_r) attacks. (iii) Robustness is typically considered to be most interesting for networks with highly heterogeneous degree distributions, so it might not be very insightful for 2D granular packings. We note, however, that we find values of R_t and R_r for our granular networks that are more than three times as large as those for the corresponding RGG ensemble (see Table III).

(18) Rent exponent p [79]: (i) Rent's rule, which was first discovered in relation to computer chip design, defines a scaling relationship between the number of external signal connections (edges) e to a block of logic and the number of connected nodes n in the block [79]:

$$e \sim n^p,\tag{A15}$$

where $p \in [0, 1]$ is the Rent exponent. (ii) The Rent exponent measures the efficiency of the physical embedding of a topological structure. (iii) Due to the physical constraints of a 2D granular packing, we expect to observe Rentian scaling with a relatively low Rent exponent (similar to that of a lattice). The theoretical minimum value that people expect for the Rent's exponent for a 2D physical lattice is $p_t = 1 - 1/D_E$ [80–82], where D_E is the Euclidean dimension of the space (e.g., two). The case $D_E = 2$ yields $p_t = 0.5$, which is consistent with empirical results on memory circuits [83]. However, the expected value of the Rent exponent might also depend on the type of physical lattice under study (e.g., a rectangular or hexagonal lattice). For our 2D granular packings, the Rent exponent is $p \approx 0.47$.

(19) Mean connection distance (mcd): (i) An edge's estimated connection distance L_{ij} is defined as the Euclidean distance between the centroids of particles i and j. (ii) The mean connection distance (mcd) is defined as the mean of all L_{ij} values in the network. (iii) The mean connection distance in a 2D granular packing is related to the number of particles, the area of the system, and particle size.

2. Diagnostics applied to force-weighted contact networks

To characterize the structure of the force-weighted networks, we used eight diagnostics: normalized strength [84,85], diversity [86], path length [87], geodesic node betweenness [57,85], geodesic edge betweenness [60], clustering coefficient [85], transitivity [88], and optimized modularity [38].

(1) Normalized Strength S' [84,85]: (i) The strength of node i is given by the column sum of the weighted adjacency matrix:

$$S_i = \sum_j W_{ij},\tag{A16}$$

and the strength of an entire weighted network $\mathbf{W}$ is the mean of S_i over all i. The normalized strength S' is

$$S_i' = \frac{S_i}{N},\tag{A17}$$

where N is the total number of nodes. (ii) Strength is a measure of how strong the connections are in a network. (iii) In the present context, normalized strength provides a measure of

the mean contact forces between particles, and we therefore expect this diagnostic to be correlated with sound propagation. Indeed, we observe this in our calculations.

(2) *Diversity V* [86]: (i) The diversity of node i is defined as the variance of the edge weights for the set of all edges that are connected to it. It is given by

$$V_i = \left[\frac{1}{N} \sum_j (W_{ij} - \langle W_i \rangle)^2 \right]^{1/2}. \tag{A18}$$

The diversity of an entire weighted network is the mean of V_i over all i. (ii) Diversity is a measure of the variance of connectivity strengths in a network. (iii) In the present context, diversity is a measure of the variance of contact forces between particles, and it has a high positive correlation with normalized strength.

(3) *Global efficiency E_w* [56]: (i) Let $d_{ij}^w = \max(W_{ij}) - W_{ij}$ be the weighted shortest path between nodes i and j. The global efficiency of node i is then defined as

$$E_w(i) = \frac{1}{N-1} \sum_{j \neq i} \frac{1}{d_{ij}^w}. \tag{A19}$$

The global efficiency E_w is the mean value of $E_w(i)$ over all nodes i. (ii) One can interpret global efficiency as a measure of how efficiently a signal is transmitted through a network. (iii) We expect the global efficiency of the force-weighted contact network to be large in the center of the packing and small on the edges of the packing because particles that are not geographically close to each other do not exert forces on one another. Indeed, this is what we observe.

(4) *Clustering coefficient C_w* [85]: (i) One can define a weighted clustering coefficient $C_w(i)$ of node i using the formula

$$C_w(i) = \frac{1}{S_i(k_i - 1)} \sum_{j,k} \frac{(W_{ij} + W_{ik})}{2} A_{ij} A_{ik} A_{jk}, \tag{A20}$$

where S_i is node i's strength, k_i is its degree, **W** is the weighted adjacency matrix, and **A** is the underlying binary adjacency matrix. (ii) The weighted clustering coefficient $C_w(i)$ measures the strength of local connectivity. (iii) The weighted clustering coefficient is constrained by the underlying contact network structure, so we expect it to have a high positive correlation with the binary clustering coefficient $C(i)$. Indeed, the Pearson correlation coefficient between the binary and weighted clustering coefficients over the experimental runs is $r \approx 0.94$ (with a p-value of $p \approx 2 \times 10^{-9}$). Both diagnostics tend to attain their highest values on the edges of the packing, where nodes' immediate neighbors are most likely to also be connected to one another.

(5) *Geodesic node betweenness B_w* [89]: (i) Geodesic betweenness is defined for the ith node in a network $\mathcal{G}$ as

$$B_w(i) = \sum_{j,m,i \in \mathcal{G}} \frac{\tilde{\psi}_{j,m}(i)}{\tilde{\psi}_{j,m}}, \tag{A21}$$

where all three nodes (j, m, and i) must be different from each other, $\tilde{\psi}_{j,m}$ denotes the number of geodesic weighted paths between nodes j and m, and $\tilde{\psi}_{j,m}(i)$ denotes the number of geodesic weighted paths between j and m that pass through node i. (As with weighted global efficiency, the weighted shortest path between nodes i and j is d_{ij}^w. Other choices for how to compute d_{ij}^w are, of course, possible.) The weighted geodesic betweenness of an entire network B_w is defined as the mean of $B_w(i)$ over all nodes i. (ii) One can interpret weighted geodesic betweenness as a measure of traffic flow on a network. (iii) We expect betweenness in weighted networks to correlate positively with strength, just as betweenness in binary networks tends to correlate positively with degree [59]. In a 2D granular packing, we expect particles in the center of the system to have high values of weighted betweenness because more paths must pass through them to connect the particles at the periphery of the system. We indeed find this to be the case.

(6) *Geodesic edge betweenness B_{ew}* [69,89]: (i) We define geodesic edge betweenness on weighted networks using the number of weighted shortest paths between pairs of nodes that are connected by an edge. (We again determine the path distance between nodes i and j using d_{ij}^w.) For the edge that connects nodes j and m, the weighted geodesic edge betweenness is

$$B_{ew}(j,m) = \sum_{i,k} \tilde{\psi}_{i,k}(j,m), \tag{A22}$$

where $\tilde{\psi}_{i,k}(j,m)$ is the number of shortest paths between nodes i and k that pass through the edge that connects nodes j and m. (ii) Weighted edge betweenness indicates the influence of an edge on traffic flow through a network. (iii) In a 2D granular packing, the edge betweenness should give an indication of the influence of a contact on a hypothetical flow through the network. We find that edge betweenness is largest in the center of the system because more paths must pass through these edges to connect all pairs of particles.

(7) *Modularity index Q_w* [36–38]: The weighted modularity of a network partition is

$$Q_w = \frac{1}{2\bar{W}} \sum_{ij} \left[W_{ij} - \frac{S_i S_j}{2\bar{W}} \right] \delta_{g_i, g_j}, \tag{A23}$$

where S_i is node i's strength, $\bar{W}$ is the total strength of the edges in a network, W_{ij} is an element of the weighted adjacency matrix, δ_{ij} is the Kronecker delta, and g_i is the label of the community to which node i has been assigned. As with unweighted networks, one uses some computational heuristic to find a partition that maximizes Q. We use the Louvain locally greedy optimization method [39]. (ii) The maximum value of Q is a measure of how well a network can be partitioned into cohesive communities. (iii) In a 2D granular packing, in which forces between particles are represented as edge weights, we expect communities to be localized in space because the forces between nodes in potential communities are constrained geographically. Indeed, as shown in Fig. 2, this is indeed the case.

(8) Transitivity T [88]: (i) The weighted transitivity $T(i)$ of node i is

$$T(i) = \frac{2}{k_i(k_i + 1)} \sum_{j,k} (\tilde{W}_{ij} \tilde{W}_{jk} \tilde{W}_{ik})^{1/3}, \qquad \text{(A24)}$$

where we have normalized weights by the maximum edge weight in the matrix:

$$\tilde{W}_{ij} = \frac{W_{ij}}{\max(W_{ij})}. \qquad \text{(A25)}$$

The transitivity T of the entire network is the mean of $T(i)$ over all nodes i. (ii) Weighted transitivity is a generalization of the local clustering coefficient (which is sometimes called "transitivity") in unweighted networks in which one computes the sum of the weights of edges in a network's triangles instead of computing simply the number of triangles. (iii) We expect weighted transitivity to be similar to the weighted clustering coefficient C_w. Indeed, we find that the two variables are highly correlated over experimental runs (with a Pearson correlation coefficient of $r \approx 0.99$ and a p-value of $p \approx 1 \times 10^{-16}$).

We implemented all computational and simple statistical operations (such as t-tests and correlations) using MATLAB® (MathWorks, Natick, MA). We estimated network diagnostics using a combination of in-house software, the Brain Connectivity Toolbox [90], the MATLAB Boost Graph Library, and the code [91] for the Louvain optimization of modularity [39] that we obtained from Peter Mucha.

APPENDIX B: RELIABILITY OF NETWORK STRUCTURE

We quantify the reliability of each diagnostic by calculating the coefficient of variation (a normalized measure of dispersion) over the 17 experimental runs: $\text{CV} = \sigma/|\mu|$, where σ is the standard deviation and μ is the mean. Values of $\text{CV} \lesssim 0.2$ are commonly considered to be acceptable, as they indicate that a variable is reliable [78,92,93]. See Table I for CV values for all binary network diagnostics and Fig. 8(b) for a corresponding bar graph. Interestingly, reliable diagnostics are dispersed among the quantities that we considered rather than focused on sets of related diagnostics.

For the force-weighted granular networks, we find lower reliability (i.e., higher values of CV) for the diagnostics than for the (binary) contact networks. Compare Figs. 8(b) to 9(b) and Table I to Table II. It is possible that the reliability is lower in the weighted networks because a large selection of force-chain networks are consistent with a given packing [94]. Therefore, for each binary network, we are sampling one weighted network out of the many possible force-chain networks that could arise from the underlying contacts. Based on this degeneracy, we might expect that network diagnostics that depend on the forces (i.e., network geometry) might be less consistent across experiments than those based on contacts (i.e., network topology) alone. As with the binary networks, the strongly reliable weighted-network diagnostics are dispersed among the various diagnostics rather than focused on sets of related quantities.

TABLE I. Reliability of network diagnostics for the (binary) contact networks. We measure reliability using coefficient of variance (CV).

Binary contact network diagnostic	Variable	CV
Mean connection distance	mcd	0.0046
Geodesic edge betweenness	B_e	0.0090
Global efficiency	E_g	0.0114
Rent exponent	p	0.0171
Random-walk node betweenness	B_{rw}	0.0176
Number of nodes	N	0.0179
Geodesic node betweenness	B	0.0213
Modularity: Louvain optimization	Q_L	0.0071
Modularity: spectral optimization	Q_s	0.0252
Closeness centrality	C_c	0.0267
Number of edges	D	0.0360
Synchronizability	s	0.0408
Robustness, random	R_r	0.0456
Clustering coefficient	C	0.0496
Subgraph centrality	C_s	0.0528
Local efficiency	E_l	0.0573
Robustness, targeted	R_t	0.0727
Communicability	C_o	0.0829
Hierarchy	h	0.1080
Eigenvector centrality	C_e	0.1150
Degree assortativity	a	0.3219

APPENDIX C: COMPARISON OF CONTACT NETWORKS TO RANDOM GEOMETRIC GRAPHS

Many of the diagnostics that we compute for the granular networks are highly correlated with one another [see Fig. 9(a)]. In the (binary) contact networks, they form roughly two families, where the correlations among the diagnostics within a given family are high. The diagnostics that we used for the weighted networks also exhibit some correlations [see Fig. 9(a)], and (unsurprisingly) this is particularly evident for diagnostics that are known to be closely related mathematically. For example, the weighted clustering coefficient is highly correlated with transitivity, and geodesic node betweenness is highly correlated with geodesic edge betweenness.

It is important to think about the possible origins of correlations between the various network diagnostics. Some of them might be specific features of the precise granular system under consideration, but others might arise because our granular packings are confined in 2D rather than in 3D or because of our

TABLE II. Reliability of network diagnostics for the force-weighted contact networks. We measure reliability using coefficient of variance (CV).

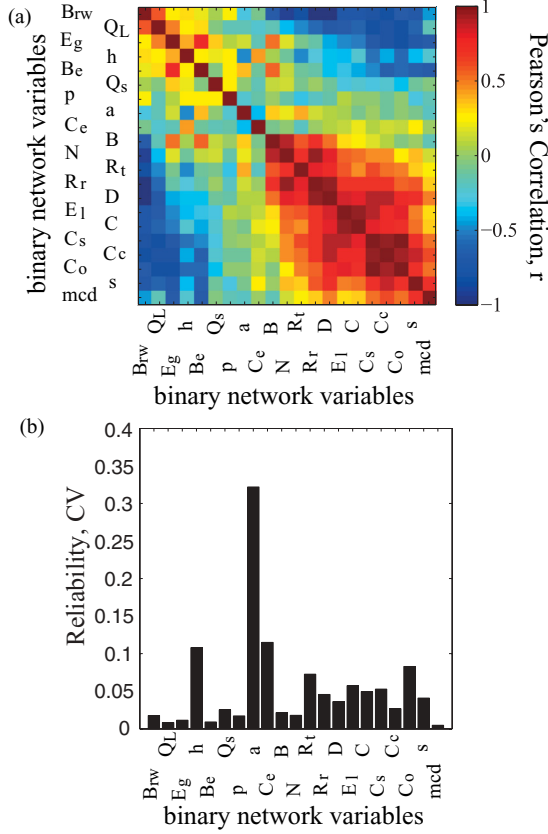| Force-weighted contact network diagnostic	Variable	CV
Transitivity	T	0.0339
Clustering coefficient	C_w	0.0549
Geodesic node betweenness	B_w	0.0282
Geodesic edge betweenness	B_{ew}	0.0199
Normalized strength	S'	0.0000
Modularity: Louvain optimization	Q_w	0.0135
Diversity	V	0.0412
Global efficiency	E_w	0.1094

FIG. 8. (Color online) (a) Relationships between 21 binary network diagnostics: degree assortativity (a), geodesic node betweenness (B), closeness centrality (C_c), clustering coefficient (C), communicability (C_o), geodesic edge betweenness (B_e), eigenvector centrality (C_e), global efficiency (E_g), hierarchy (h), local efficiency (E_l), modularity optimized using the Louvain (Q_L) and spectral (Q_s) heuristics, number of nodes (N), number of edges (D), mean connection distance (mcd), random-walk node betweenness (B_{rw}), Rent exponent (p), robustness to random attack (R_r), robustness to targeted attack (R_t), subgraph centrality (C_s), and synchronizability (s). We order the diagnostics to maximize the correlation along the diagonal for better visualization of highly correlated groups of diagnostics. Color indicates the correlation between global network diagnostics over the 17 experimental runs. (b) Reliability, as measured by the coefficient of variation (CV), over the 17 runs for the 21 binary network diagnostics reported in panel (a).

FIG. 9. (Color online) (a) Relationships between eight diagnostics applied to the weighted networks: geodesic node betweenness (B_w), clustering coefficient (C_w), diversity (V), geodesic edge betweenness (B_{ew}), global efficiency (E_w), modularity (Q_w) optimized using the Louvain method, and normalized strength (S'). We ordered the diagnostics to maximize the correlation along the diagonal for better visualization of highly correlated groups. Color indicates the correlation between global network diagnostics over the 17 experimental runs. (b) Reliability, as measured by the coefficient of variation (CV), over the 17 runs for the eight weighted graph diagnostics reported in panel (a).

particular preparation protocol. Still others might be general properties of spatially embedded systems (in any dimension), of granular materials, or of networks in general.

To examine such issues, it is desirable to compare network diagnostics computed for the networks obtained from experimental data with those obtained from appropriate ensembles of null-model networks. It is common to compare the structures of networks under study to those that would be expected in Erdős-Rényi random graphs or from some other random-graph ensemble [1]. The networks that we study in the present paper—namely, contact networks in granular packings—are spatially embedded (in the plane) because of physical constraints. The development of null models is a wide open area of research for spatially embedded networks [8], but we can make some progress for the binary
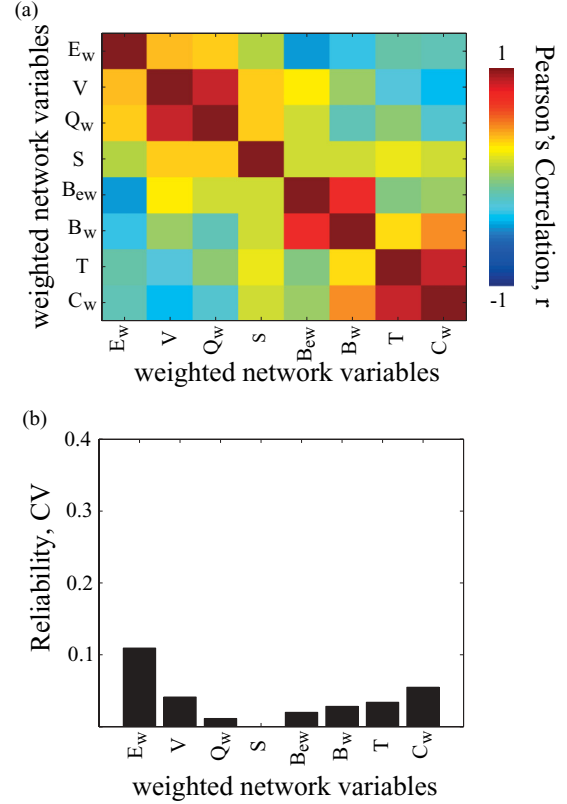
contact networks by comparing the network diagnostics in those networks to computations of the same diagnostics using an ensemble of random geometric graphs (RGGs). As we will now discuss, we find that all diagnostics (except for the ones that we fix when defining the RGG ensemble to correspond to their counterparts in the real networks) are significantly different in the real versus the random networks.

The simplest RGG [8,32,95] contains N nodes that are randomly distributed according to some probability distribution throughout an ambient space, which in our case is $\mathbb{R}^2$ [97]. One then places an edge between any pair of nodes i and j that are separated by a distance of at most $2r$, where one should think of the parameter r as the radius of a ball (using some metric) in the confining space. In planar Euclidean space, one considers a disk in $\mathbb{R}^2$ and uses ordinary (Euclidean) distance.

To compare the networks that we study to RGGs, we generated RGGs in which we placed nodes randomly and uniformly within the 2D space of the granular packing. For each experimental run, we create an ensemble of 100 RGGs in which the number of nodes is identical to that in the experimental system. We likewise fix the number of edges (D) in each RGG to be identical to that in the real system by

TABLE III. Comparison of binary network diagnostics in the (real) experimental graphs (EGs) and the random geometric graphs (RGGs). We show the mean values of the EGs (column 1), the mean values of the RGGs (column 2), the t-values (column 3), and p-values (column 4) for a two-sample t-test between the network-diagnostic values for the two families of networks (EGs and RGGs).

Diagnostic name	EG	RGG	t	p
EG less than RGG				
Local efficiency	0.33	0.67	73.33	3.1×10^{-37}
Modularity: Louvain optimization	0.81	0.92	70.52	7.2×10^{-36}
Clustering coefficient	0.26	0.54	85.28	2.5×10^{-30}
Random-walk betweenness	0.09	0.20	39.73	8.2×10^{-29}
Degree assortativity	0.14	0.57	38.52	2.2×10^{-28}
Subgraph centrality	7.19	28.79	22.41	3.9×10^{-21}
Communicability	0.15	0.73	17.79	3.6×10^{-18}
Rent exponent	0.47	0.50	15.41	2.2×10^{-16}
EG greater than RGG				
Global efficiency	0.10	0.03	94.41	1.0×10^{-40}
Mean connection distance	39.60	32.32	79.38	2.5×10^{-38}
Robustness, random	8.38×10^4	2.33×10^4	54.89	3.0×10^{-33}
Closeness centrality	7.84	4.47	50.29	4.9×10^{-32}
Synchronizability	0.0014	0.0004	44.71	2.2×10^{-30}
Robustness, targeted	7.08×10^4	1.96×10^4	36.96	7.9×10^{-28}
Edge betweenness	13.33	4.55	34.71	5.6×10^{-27}
Geodesic node betweenness	6.24×10^3	2.16×10^3	30.95	2.0×10^{-25}
Hierarchy	0.76	0.27	24.42	2.9×10^{-22}
Eigenvector centrality	0.0172	0.0080	19.15	4.2×10^{-19}
Modularity: spectral optimization	0.78	0.75	5.06	1.6×10^{-5}

choosing the threshold $2r$ so that the number of inter-node distances less than $2r$ is equal to D. We calculate the other 19 binary diagnostics (i.e., except for the number of nodes and the number of edges, as those have been fixed to be equal in the two sets of networks) and compute their mean over the 100 RGGs in each ensemble. By performing these computations for each experimental run, we create one estimate of each of the 19 diagnostic values for each of the 17 runs. We report in Table III the mean values for both the real networks and the networks generated from the RGG ensembles. We also report t-values

and p-values for two-sample t-tests between the values in the 17 real networks and the 17 mean values in the RGG networks. As we show in Table III, each of the 19 network diagnostics is significantly different between the two groups. Measures of local connectivity (e.g., clustering coefficient) are higher in the RGG, whereas measures of global connectivity and physical distance are lower. These results illustrate that the networks in the RGG ensemble have more locally connected structures than those in the 2D granular system under study.

[1] M. E. J. Newman, *Networks: An Introduction* (Oxford University Press, Oxford, 2010).

[2] M. van Hecke, J. Phys.: Condens. Matter **22**, 033101 (2010).

[3] A. J. Liu and S. R. Nagel, Annu. Rev. Condens. Matter Phys. **1**, 347 (2010).

[4] M. Oda, Soils Foundations **12**, 17 (1972).

[5] M. Oda, S. Nemat-Nasser, and M. Mehrabadi, Earthq. Res. Engn. Lab. Tech. Report, 804 (1980).

[6] M. Oda, Soils Foundations **22**, 96 (1982).

[7] H. Jaeger, S. Nagel, and R. P. Behringer, Rev. Mod. Phys. **68**, 1259 (1996).

[8] M. Barthélemy, Phys. Rep. **49**, 1 (2011).

[9] M. Herrera, S. McCarthy, S. Slotterback, E. Cephas, W. Losert, and M. Girvan, Phys. Rev. E **83**, 061303 (2011).

[10] D. M. Walker and A. Tordesillas, Int. J. Solids Struct. **47**, 624 (2010).

[11] C. H. Liu, S. R. Nagel, D. A. Schecter, S. N. Coppersmith, S. Majumdar, O. Narayan, and T. A. Witten, Science **269**, 513 (1995).

[12] D. Howell, R. P. Behringer, and C. Veje, Phys. Rev. Lett. **82**, 5241 (1999).

[13] V. F. Nesterenko, *Dynamics of Heterogeneous Materials* (Springer-Verlag, New York, 2001).

[14] P. J. Digby, J. Appl. Mech. **48**, 803 (1981).

[15] J. D. Goddard, Proc. Royal Soc. A **430**, 105 (1990).

[16] B. Velický and C. Caroli, Phys. Rev. E **65**, 021307 (2002).

[17] E. Somfai, J.-N. Roux, J. Snoeijer, M. van Hecke, and W. van Saarloos, Phys. Rev. E **72**, 021301 (2005).

[18] C. H. Liu, Phys. Rev. B **50**, 782 (1994).

[19] X. Jia, C. Caroli, and B. Velicky, Phys. Rev. Lett. **82**, 1863 (1999).

[20] H. A. Makse, N. Gland, D. L. Johnson, and L. M. Schwartz, Phys. Rev. Lett. **83**, 5070 (1999).

[21] H. A. Makse, N. Gland, D. L. Johnson, and L. Schwartz, Phys. Rev. E **70**, 061302 (2004).

[22] E. T. Owens and K. E. Daniels, Europhys. Lett. **94**, 54005 (2011).

[23] L. Kondic, A. Goullet, C. S. O'Hern, M. Kramar, K. Mischaikow, and R. P. Behringer, Europhys. Lett. **97**, 54001 (2012).

[24] P. Ronhovde, S. Chakrabarty, D. Hu, M. Sahu, K. K. Sahu, K. F. Kelton, N. A. Mauro, and Z. Nussinov, Eur. Phys. J. B **34**, 105 (2011).

[25] A. N. Lazaridi and V. F. Nesterenko, Prikl. Mekh. Tekh. Fiz. **26**, 115 (1985).

[26] C. Coste, E. Falcon, and S. Fauve, Phys. Rev. E **56**, 6104 (1997).

[27] S. Job, F. Melo, A. Sokolow, and S. Sen, Phys. Rev. Lett. **94**, 178002 (2005).

[28] N. Boechler, G. Theocharis, S. Job, P. G. Kevrekidis, M. A. Porter, and C. Daraio, Phys. Rev. Lett. **104**, 244302 (2010).

[29] G. Huillard, X. Noblin, and J. Rajchenbach, Phys. Rev. E **84**, 016602 (2011).

[30] H. A. Janssen, Z. Ver. Deut. Ing. **39**, 1045 (1895).

[31] T. S. Majmudar, M. Sperl, S. Luding, and R. Behringer, Phys. Rev. Lett. **98**, 058001 (2007).

[32] M. Penrose, *Random Geometric Graphs* (Oxford University Press, Oxford, 2003).

[33] S. Ostojic, E. Somfai, and B. Nienhuis, Nature (London) **439**, 828 (2006).

[34] J. Reichardt and S. Bornholdt, Phys. Rev. E **74**, 016110 (2006).

[35] S. Fortunato and M. Barthélemy, Proc. Natl. Acad. Sci. USA **104**, 36 (2007).

[36] S. Fortunato, Phys. Rep. **486**, 75 (2010).

[37] M. A. Porter, J.-P. Onnela, and P. J. Mucha, Not. Am. Math. Soc. 0**56**, 1082 (2009).

[38] M. E. J. Newman and M. Girvan, Phys. Rev. E **69**, 026113 (2004).

[39] V. D. Blondel, J. L. Guillaume, R. Lambiotte, and E. Lefebvre, J. Stat. Mech. (2008) P10008.

[40] J. Reichardt and S. Bornholdt, Phys. Rev. Lett. **93**, 218701 (2004).

[41] J.-P. Onnela, D. J. Fenn, S. Reid, M. A. Porter, P. J. Mucha, M. D. Fricker, and N. S. Jones, Phys. Rev. E **86**, 036104 (2012).

[42] P. Schall and M. van Hecke, Annu. Rev. Fluid Mech. **42**, 67 (2010).

[43] M. Wyart, Ann. Phys. **30**, 1 (2005).

[44] M. E. J. Newman, Proc. Natl. Acad. Sci. USA **103**, 8577 (2006).

[45] U. Brandes, D. Delling, M. Gaertler, R. Goerke, M. Hoefer, Z. Nikoloski, and D. Wagner, IEEE Trans. Know. Data Eng. **20**, 172 (2008).

[46] B. H. Good, Y. A. de Montjoye, and A. Clauset, Phys. Rev. E **81**, 046106 (2010).

[47] L. Kuncheva and S. Hadjitodorov, IEEE Intl. Conf. Sys. Man. Cyber. **2**, 1214 (2004).

[48] L. Danon, J. Duch, A. Díaz-Guilera, and A. Arenas, J. Stat. Mech. (2005) P09008.

[49] R. Guimerà and L. A. N. Amaral, Nature (London) **433**, 895 (2005).

[50] M. Saadatfar, A. P. Sheppard, T. J. Senden, and A. J. Kabla, J. Mech. Phys. Solids **60**, 55 (2012).

[51] S. Mukhopadhyay and J. Peixinho, Phys. Rev. E **84**, 011302 (2011).

[52] M. Wyart, L. E. Silbert, S. R. Nagel, and T. A. Witten, Phys. Rev. E **72**, 051306 (2005).

[53] S. Henkes, M. van Hecke, and W. van Saarloos, Europhys. Lett. **90**, 14003 (2010).

[54] M. L. Falk and J. S. Langer, Phys. Rev. E **57**, 7192 (1998).

[55] M. L. Manning and A. J. Liu, Phys. Rev. Lett. **107**, 108302 (2011).

[56] V. Latora and M. Marchiori, Phys. Rev. Lett. **87**, 198701 (2001).

[57] L. C. Freeman, Sociometry **40**, 35 (1977).

[58] Betweenness centrality is often called simply "betweenness," so we will do this in the remainder of this paper.

[59] M. E. J. Newman, Soc. Netw. **27**, 39 (2005).

[60] M. Girvan and M. E. J. Newman, Proc. Natl. Acad. Sci. USA **99**, 7821 (2002).

[61] P. Bonacich, J. Math. Soc. **2**, 113 (1972).

[62] G. Sabidussi, Psychometrika **31**, 581 (1966).

[63] E. Estrada and J. A. Rodríguez-Velázquez, Phys. Rev. E **71**, 056103 (2005).

[64] E. Estrada and N. Hatano, Phys. Rev. E **77**, 036111 (2008).

[65] P. Bonacich, Amer. J. Soc. **92**, 1170 (1987).

[66] D. J. Watts and S. H. Strogatz, Nature (London) **393**, 440 (1998).

[67] E. Ravasz and A.-L. Barabási, Phys. Rev. E **67**, 026112 (2003).

[68] M. Barahona and L. M. Pecora, Phys. Rev. Lett. **89**, 054101 (2002).

[69] M. E. J. Newman, Phys. Rev. Lett. **89**, 208701 (2002).

[70] R. Albert, H. Jeong, and A. L. Barabási, Nature (London) **406**, 378 (2000).

[71] B. S. Landman and R. L. Russo, IEEE Trans. Comput. **C-20**, 1469 (1971).

[72] D. S. Bassett, E. T. Bullmore, B. A. Verchinski, V. S. Mattay, D. R. Weinberger, and A. Meyer-Lindenberg, J. Neurosci. **28**, 9239 (2008).

[73] P. Bonacich, Social Meth. **4**, 176 (1972).

[74] C. Dangalchev, Physica A **365**, 556 (2006).

[75] M. E. J. Newman, SIAM Rev. **45**, 167 (2003).

[76] S. Achard, R. Salvador, B. Whitcher, J. Suckling, and E. Bullmore, J. Neurosci. **26**, 63 (2006).

[77] M. E. Lynall, D. S. Bassett, R. Kerwin, P. McKenna, U. Muller, and E. T. Bullmore, J. Neurosci. **30**, 9477 (2010).

[78] D. S. Bassett, J. A. Brown, V. Deshpande, J. M. Carlson, and S. T. Grafton, NeuroImage **54**, 1262 (2011).

[79] P. Christie and D. Stroobandt, IEEE Trans. VLSI Syst. **8**, 639 (2000).

[80] H. M. Ozaktas, Opt. Eng. **31**, 1563 (1992).

[81] D. S. Bassett, D. L. Greenfield, A. Meyer-Lindenberg, D. R. Weinberger, S. Moore, and E. Bullmore, PLoS Comput. Biol. **6**, e1000748 (2010).

[82] P. Verplaetse, J. Dambre, D. Stroobandt, and J. Van Campenhout, in *Proceedings of the 2001 International Workshop on System-Level Interconnect Prediction*, SLIP '01 (ACM, New York, NY, 2001), pp. 33–40.

[83] R. L. Russo, IEEE Trans. Comput. **C-21**, 147 (1972).

[84] S. Horvath, *Weighted Network Analysis: Applications in Genomics and Systems Biology* (Springer-Verlag, New York, 2011).

[85] A. Barrat, M. Barthélemy, R. Pastor-Satorras, and A. Vespignani, Proc. Natl. Acad. Sci. USA **101**, 3747 (2004).

[86] K. E. Campbell, P. V. Marsden, and J. S. Hurlbert, Social Netw. **8**, 97 (1986).

[87] E. W. Dijkstra, Num. Math. **1**, 269 (1959).

[88] J.-P. Onnela, J. Saramäki, J. Kertész, and K. Kaski, Phys. Rev. E **71**, 065103 (2005).

[89] K. Park, Y.-C. Lai, and N. Ye, Phys. Rev. E **70**, 026109 (2004).

[90] M. Rubinov and O. Sporns, NeuroImage **52**, 1059 (2009).

[91] I. S. Jutla, L. G. S. Jeub, and P. J. Mucha (2012), http://netwiki.amath.unc.edu/GenLouvain.

[92] L. Deuker, E. T. Bullmore, M. Smith, S. Christensen, P. J. Nathan, B. Rockstroh, and D. S. Bassett, NeuroImage **47**, 1460 (2009).

[93] L. A. Mancl, P. P. Hujoel, and T. A. DeRouen, J. Dent. Res. **83**, C95 (2004).

[94] J. H. Snoeijer, T. J. H. Vlugt, M. van Hecke, and W. van Saarloos, Phys. Rev. Lett. **92**, 054302 (2004).

[95] J. Dall and M. Christensen, Phys. Rev. E **66**, 016121 (2002).

[96] C. McDiarmid, A. Steger, and D. J. Welsh, J. Comb. Theory, Ser. B **93**, 187 (2005).

[97] Note that a "random geometric graph" in two dimensions is a different mathematical object from what is known as a "random planar graph" [96].

Erratum: Influence of network topology on sound propagation in granular materials [Phys. Rev. E 86, 041306 (2012)]

Danielle S. Bassett, Eli T. Owens, Karen E. Daniels, and Mason A. Porter

Computations. In our paper, some of our computations were for quantities that were similar to those that we reported in our formulas, but they were not quite the same. Below we provide the corrected formulas.

For weighted networks, we calculated a local version of a clustering coefficient. [See Eq. (A20) on p. 12 of our paper.] Let k_i be the (unweighted) degree of node i, and let $\hat{\mathbf{W}}$ denote the weighted adjacency matrix. The contribution $N_{\text{cyc}_3}(i)$ from length-3 cycles that include node i is equal to the (i,i)th element of the matrix $\hat{\mathbf{W}}$, where

$$\hat{\mathbf{W}} = \mathbf{Y}^3,$$
$$Y_{ij} = W_{ij}^{1/3}, \qquad i,j \in \{1,\ldots,N\}. \tag{1}$$

We then calculated a local weighted clustering coefficient,

$$C_w(i) = \frac{N_{\text{cyc}_3}(i)}{k_i(k_i - 1)}, \tag{2}$$

for all nodes i that are part of at least one 3-cycle. For any node i that is not part of a 3-cycle, we set $C_w(i) = 0$. The code (CLUSTERING_COEF_WU.M) that we used for this computation comes from the Brain Connectivity Toolbox [1]. To subsequently calculate a global weighted clustering coefficient, we computed $C_w = \frac{1}{N}\sum_i C_w(i)$.

For weighted networks, we also calculated a second type of global clustering coefficient. [See Eq. (A24) on p. 13 of our paper.] We computed $N_{\text{cyc}_3}(i)$ as above, and we then calculated a global weighted transitivity using the formula

$$T = \frac{\sum_i N_{\text{cyc}_3}(i)}{\sum_i k_i(k_i - 1)} \tag{3}$$

for all nodes i. The code (TRANSITIVITY_WU.M) that we used for this computation comes from the Brain Connectivity Toolbox [1].

Typographical errors. Our formula [see Eq. (A2) on p. 9 of the paper] for the geodesic node betweenness centrality of node i in an unweighted network should read

$$B_i = \sum_{j,m \in \mathcal{G}} \frac{\psi_{j,m}(i)}{\psi_{j,m}}, \tag{4}$$

where all three nodes (j, m, and i) must be different from each other, $\psi_{j,m}$ is the number of geodesic paths between nodes j and m, and $\psi_{j,m}(i)$ is the number of geodesic paths between j and m that traverse node i. Our computations of node betweenness for unweighted networks in the paper used Eq. (4), but the equation in our paper makes it look like we were summing over i. That is not the case, as there is a value of geodesic node betweenness for each node i. The same change corrects our equation [see Eq. (A21) on p. 12 of the paper] for geodesic node betweenness centrality in a weighted network, and again all computations in our paper used the correct equation. The code (BETWEENNESS_BIN.M and BETWEENNESS_WEI.M) that we used for this computation comes from the Brain Connectivity Toolbox [1].

Our formula [see Eq. (A3) on p. 9 of the paper] for the geodesic edge betweenness centrality of edge (j,m) that connects nodes j and m in an unweighted network should read

$$B_e(j,m) = \sum_{i,k} \frac{\psi_{i,k}(j,m)}{\psi_{j,m}}, \tag{5}$$

where $\psi_{j,m}$ is again the number of geodesic paths between nodes j and m, and $\psi_{i,k}(j,m)$ is the number of geodesic paths between i and k that traverse the edge that connects nodes j and m. That is, we used the same type of normalization as in our computation of geodesic node betweenness centrality. The same comment about normalization applies to our equation [see Eq. (A22) on p. 12 of the paper] for geodesic edge betweenness centrality in a weighted network. The code (EDGE_BETWEENNESS_BIN.M and EDGE_BETWEENNESS_WEI.M) that we used for this computation comes from the Brain Connectivity Toolbox [1].

In our equation [see Eq. (A10) on p. 10 of the paper] for the local efficiency of node i in an unweighted network, we neglected to state explicitly that N_{G_i} represents the number of nodes in the subgraph G_i.

As we noted earlier in this Erratum, our formula [see Eq. (A24) on p. 13] for the global transitivity in a weighted network should read

$$T = \frac{\sum_i N_{\mathrm{cyc}_3}(i)}{\sum_i k_i(k_i - 1)} \qquad (6)$$

for all nodes i. The code (TRANSITIVITY_WU.M) that we used for this computation comes from the Brain Connectivity Toolbox [1]. The difference from the formula [see Eq. (A24) on p. 13] in our paper is that the denominator should be $k_i(k_i - 1)$ rather than $k_i(k_i + 1)$. All of the computations in our paper used the correct factor [i.e., $k_i(k_i - 1)$] in the denominator.

Finally, as a trivial correction, the phrase "edge-connecting node i and node j" on p. 3 should instead read "edge that connects nodes i and j" (i.e., there should not be any hyphen).

Acknowledgments. We thank J. Setford for his help in uncovering several of the above issues.

---

[1] M. Rubinov and O. Sporns, *Brain Connectivity Toolbox* (2010), https://sites.google.com/site/bctnet/.